Dimmable Proximity-Based Indoor Visible Light Positioning with Interference Mitigation

Poompat Saengudomlert†, Member,
Karel L. Sterckx, and **Nutthakun Wannaprapa**, Non-members

ABSTRACT

This work presents a development of a dimmable proximity-based indoor Visible Light Positioning (VLP) system. Light Emitting Diode (LED) lamps are used to transmit position numbers, which are detected by a mobile receiver containing a Photo Diode (PD). For data transmissions, Pulse Position Modulation (PPM) and inverse PPM (IPPM) are used to provide low and high illumination levels. To mitigate signal interference between adjacent LED lamps, timeslot-interleaved Time Division Multiplexing (TDM) is applied so that adjacent LED lamps transmit in disjoint sets of timeslots. Simulation experiments are conducted for LED lamps 1.5 m apart on the ceiling of height 2 m, with the receiver 0.5 m above the floor and the Signal-to-Noise Ratio (SNR) below each lamp equal to 20 dB. For the same illumination level, TDM can reduce the detection error percentages around the midpoint approximately from 80% to 40%. For different illumination levels, TDM does not reduce peak errors at the midpoint but shortens the position interval with errors above 10% from approximately 0.5 m to approximately 0.25 m. Finally, hardware implementation and experiments are presented to demonstrate the potential of the proposed dimmable proximity-based VLP system.

Keywords: Visible Light Positioning, Light Dimming, Pulse Position Modulation, Detection Error

1. INTRODUCTION

Compared to outdoor positioning, for which Global Positioning System (GPS) has been widely used, indoor positioning remains a relatively open problem. While various Radio Frequency (RF) signals can be used as reference signals for positioning, optical signals from Light Emitting Diode (LED) lamps can provide an attractive alternative since in most places LED lamps are already installed on the ceilings for illumination purposes. Indoor positioning based on reference signals from LED lamps is referred to as Visible Light Positioning (VLP) [1–4].

For typical indoor environments, the illumination below each LED lamp on the ceiling is limited to a coverage radius of a few meters. For basic object tracking applications, including informing a human user his or her current position, it is sufficient to know the position number of the closest LED lamp. This approach of positioning is referred to as proximity-based VLP [2–4]. As a potential application, proximity-based VLP can be integrated with a map database and a routing algorithm to create an indoor pedestrian navigation system.

For data transmissions using visible light, Pulse Position Modulation (PPM) and its variants have been adopted in industrial standards [5, 6]. In M-PPM, data bits are represented as the presence of a pulse in one of M timeslots in a symbol period. In M-inverse PPM (M-IPPM), the absence instead of the presence of a pulse in one of M timeslots is used to represent data bits. Since LEDs are incoherent light sources, PPM based signal transmissions rely on Intensity Modulation (IM) at a transmitter and Direct Detection (DD) at a receiver [7, 8].

For the sake of energy savings when natural light is sufficient as well as human comfort when low illumination levels are preferred, light dimming is an important feature and has been considered by several researchers [9, 10]. In particular, dimming support using PPM and its variants has been investigated [11–15]. In [11], throughput and Bit Error Rate (BER) performance analyses were carried out for M-PPM (low illumination level) and for M-IPPM (high illumination level) with different values of M.

In [12], different dimming levels are achieved by varying the number of pulses in each symbol period, with data bits represented by the positions of pulses. In addition, a relationship between assigning multiple pulses to represent data bits and the design of binary codes with fixed Hamming weights (fixed number of 1s) is mentioned. In [13, 14], advanced binary coding and decoding algorithms are developed and proposed for dimming support.

However, in [11–14], it is assumed that a receiver is informed which modulation scheme is being used by a transmitter. For proximity-based VLP scenarios in which a receiver is moving, the knowledge of modulation scheme will incur a large transmission overhead when compared with a small amount of data bits used to specify

Manuscript received on March 30, 2025; revised on May 8, 2025; accepted on May 19, 2025. This paper was recommended by Associate Editor Kampol Woradit.

The authors are with School of Engineering, Bangkok University, Thailand.

†Corresponding author: poompat.s@bu.ac.th

Digital Object Identifier: 10.37936/ecti-eec.2525232.258545

LED position numbers. In addition, advanced coding and decoding algorithms rely on large data frames, which are not suitable for proximity-based VLP for which small data frames are sufficient.

In [15], a flexible dimming scheme based on time sharing between PPM and IPPM is proposed for proximity-based VLP such that the receiver can detect data bits without knowing whether PPM or IPPM is being used. The associated dimming capability and BER performance analyses are provided. However, no hardware demonstration based on the proposed scheme has been reported and no consideration is given on signal interference between adjacent LED lamps.

This work presents a development of a proximity-based VLP system based on the flexible dimming scheme proposed in [15], which is extended to take into account signal interference between adjacent LED lamps. In particular, interference mitigation based on timeslot-interleaved Time Division Multiplexing (TDM) is adopted and evaluated. Numerical choices of system parameters are explained. In addition, hardware implementation of the proposed system using low-cost and commercially available components is discussed. System performances are evaluated in terms of error percentages in detecting LED position numbers. Numerical results indicate that the proposed VLP system can be practical. Note that three-dimensional positioning and tracking, while being useful for applications such as robot control, is not considered for proximity-based VLP in this work, and has been separately investigated in [16, 17].

The remaining sections are as follows. Section 2 presents the system design that includes the proposed signal modulation scheme with both dimming and interference mitigation techniques. The corresponding detection of data symbols is also discussed. Section 3 discusses simulation experiments to evaluate detection error performances. Hardware components and the development of an experimental setup are discussed in Section 4, together with experimental results for system demonstration. Finally, conclusion is made in Section 5.

2. SYSTEM DESIGN

The usage scenario of proximity-based indoor VLP is illustrated in Fig. 1. LED lamps are installed on the ceiling along a walkway, and repeatedly transmit their position numbers.

A mobile user with a handheld receiver moves along a walkway. The receiver with a PD detects the position number of the closest LED lamp. However, as indicated in Fig. 1, there are some receiver positions in overlapped coverages of adjacent LED lamps. At these positions, the receiver may fail to detect a position number correctly due to signal interference. In particular, significant interference can lead to data frame synchronization errors as well as detected bit errors, both of which lead to positioning errors. This interference problem is most severe around positions that are equidistant from their two closest LED lamps.

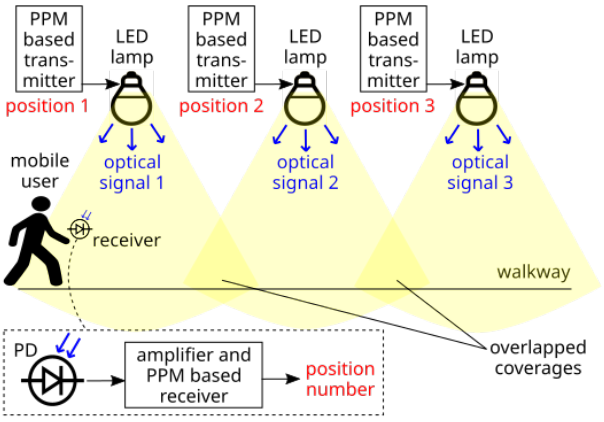

***Fig. 1**: Usage scenario of proximity-based VLP.*

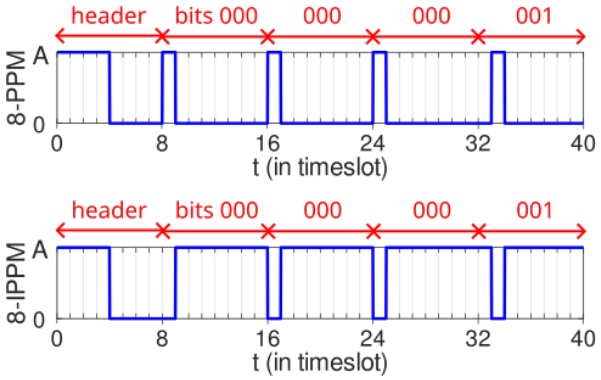

***Fig. 2**: Data frame structure for 8-PPM/IPPM without TDM. The 12 data bits are assumed to be 000 000 000 001.*

2.1 Signal Modulation

LED transmitters employ a combination of 8-PPM and 8-IPPM as proposed in [15] for dimming support. In addition, timeslot-interleaved TDM is employed between adjacent LED transmitters to mitigate signal interference in overlapped LED coverages. More specifically, adjacent LEDs transmit signals in two disjoint sets of timeslots, e.g., odd-numbered and even-numbered timeslots. Therefore, their signals do not overlap in the time domain, and signal interference is mitigated.

For ease of understanding, Fig. 2 shows the data frame structure without TDM in two cases: 8-PPM for the low illumination level and 8-IPPM for the high illumination level. In 8-PPM, each symbol period contains 8 timeslots, with a pulse signal in exactly 1 out of 8 timeslots. In 8-IPPM, each symbol period also contains 8 timeslots, but with the absence of a pulse in exactly 1 out of 8 timeslots. With more pulse signals per symbol, 8-IPPM signals have higher average values, leading to higher LED drive currents and hence higher illumination levels. Despite different illumination levels, their BER performances are known to be the same due to the same distances between data symbols in the signal space [15].

Each data frame starts with a header that lasts for 8 timeslots, with the ON signal value, denoted by A, in

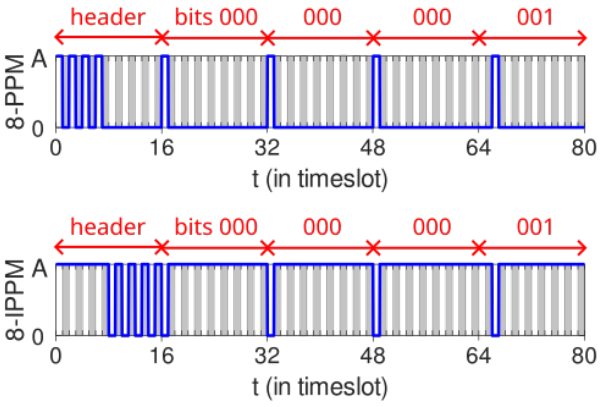

***Fig. 3**: Data frame structure for 8-PPM/IPPM with TDM. The 12 data bits are assumed to be 000 000 000 001. Idle timeslots, used by adjacent LED lamps, are indicated by shaded timeslots.*

the first 4 timeslots. Four 8-PPM/IPPM symbols follow, carrying a total of 12 bits. All 12 bits are used for position numbers in this work, but error control coding can also be applied at the expense of a few data bits. In addition, while 12 bits are sufficient in this work, it is straightforward to extend to more than 12 bits.

Fig. 3 shows the proposed data frame structure with TDM in two cases: 8-PPM and 8-IPPM. The shaded timeslots indicate idle slots to be used by adjacent LED lamps to transmit their data. Timeslots are divided into two disjoint sets, namely odd-numbered and even-numbered timeslots. Adjacent LED lamps transmit using different sets of timeslots. For 8-PPM, an LED transmitter sets the signal value to OFF during idle slots while adjacent LEDs transmit their data signals. On the other hand, for 8-IPPM, an LED transmitter sets the signal value to ON during idle slots. These OFF and ON signal values during idle slots are selected to provide low and high illumination levels for 8-PPM and 8-IPPM, respectively. It is worth noting that, since PPM/IPPM symbol detection is not affected by changing the signal mean [15], these constant signals during idle slots do not interfere with data signals from adjacent LED transmitters.

2.2 Illumination Percentages and Flickering Avoidance

Considering the always ON signal (with no data modulation) to correspond to the highest illumination level of 100%. In comparison, the percentages of illumination for 8-PPM and 8-IPPM with TDM in Fig. 3 are computed based on the fractions of ON timeslots in each data frame as follows.

$$I_{8-\text{PPM}} = \frac{8}{80} \times 100\% = 10\% \tag{1}$$

$$I_{8-\text{IPPM}} = \frac{80-8}{80} \times 100\% = 90\% \tag{2}$$

The difference between the two illumination levels of 90% − 10% = 80% can be observed and are sufficiently different for light dimming. The choice of M for M-PPM/IPPM can also vary, with the corresponding low and high illumination levels computed in the same fashion as for (1)–(2).

The timeslot duration is set to 0.2 ms in this work to prevent light flickering, as explained next. It is known that flickering will not be observed when the LED switching frequency is above 200 Hz [8]. With 8-PPM/IPPM and TDM, during data transmissions, the LED is switched on and off only once in every 16 timeslots, as shown in Fig. 3. Accordingly, the LED switching frequency, denoted by f_{LED}, is approximately equal to

$$f_{\text{LED}} \approx \frac{1}{16 \times 0.2 \text{ ms}} = 312.5 \text{ Hz}, \tag{3}$$

which is sufficiently high to avoid light flickering. More generally, for M-PPM/IPPM with timeslot duration T_s, the condition for no light flickering is $1/(2MT_s) > 200$ Hz.

2.3 Frame and Symbol Detection

Detection of LED position numbers is performed in two phases: frame header detection and data symbol detection. For frame header detection, the received signal is first sampled at the rate of 25 kHz, which for a 0.2-ms timeslot yields 5 sample/timeslot. Then, the frame header ending is found through maximizing the correlation value with the header mask signal, as illustrated in Fig. 4 for 8-PPM. It is worth noting that, due to timeslot-interleaved TDM, the mask signal contains values at non-consecutive sample indices. Fig. 5 illustrates the header search using the maximum correlation for 8-IPPM.

Without noise, frame header detection will be error-free, except at positions half-way between two adjacent LED lamps where the maximum correlation values with respect to two LED lamps are equal. With noisy received signals, a frame header detection can occur when the correlation with respect to the adjacent LED lamp is higher, leading to detecting the adjacent position number instead. When the noise level is high, a frame header detection error can also come from having the maximum correlation in the data bit section of a frame instead of in the header section.

Given a correct frame header detection, data symbol detection is based on matched filter outputs each of which corresponds to the average sample value for each timeslot. Consider a particular 8-PPM/IPPM symbol of interest. Let $R_0, ..., R_7$ denote the matched filter outputs corresponding to its eight timeslots, which are numbered as $0, ..., 7$. In addition, denote the sum and the maximum of eight matched filter outputs by

$$R_{\text{total}} = R_0 + ... + R_7, \tag{4}$$

$$R_{\max} = \max\left(\mathrm{R}_0, ..., \mathrm{R}_7\right). \tag{5}$$

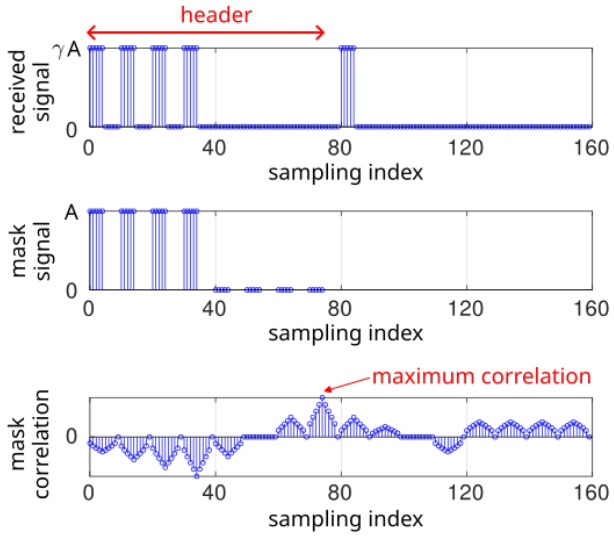

***Fig. 4**: Header search in the case of 8-PPM using the maximum correlation with the header mask signal, with only the first 32 timeslots of a data frame shown and assuming that the received signal is the transmitted signal attenuated by a factor γ.*

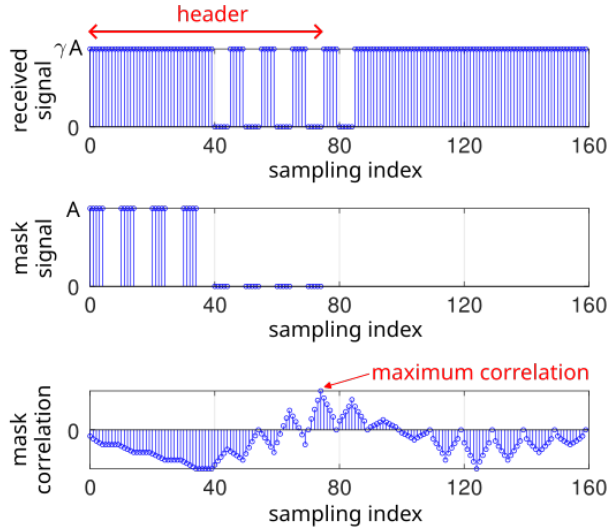

***Fig. 5**: Header search using the maximum correlation with the header mask signal, but with 8-IPPM instead of 8-PPM.*

As in [15], each 8-PPM/IPPM symbol is assigned two separate signal points based on PPM and IPPM, respectively. For example, data bits 000 are mapped to one of the following two signal points: $(A, 0, 0, 0, 0, 0, 0, 0)$ and $(0, A, A, A, A, A, A, A)$ for the low and high illumination levels, respectively. As another example, data bits 001 are mapped to one of the following: $(0, A, 0, 0, 0, 0, 0, 0)$ and $(A, 0, A, A, A, A, A, A)$.

With Additive White Gaussian Noise (AWGN), optimal symbol detection is based on the minimum-distance decision rule, taking into account the path loss γ. For example, if the Euclidean distance from $\left(\boldsymbol{R}_0, ..., \boldsymbol{R}_7\right)$ to either $\gamma\,(A, 0, 0, 0, 0, 0, 0, 0)$ or $\gamma\,(0, A, A, A, A, A, A, A)$ is

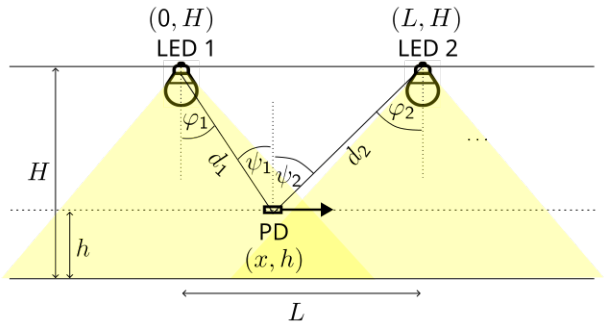

***Fig. 6**: Transmitter and receiver positions for simulation experiments.*

the minimum compared to the distances to the other signal points, then the receiver maps $\left(\boldsymbol{R}_0, ..., \boldsymbol{R}_7\right)$ to data bits 000.

The expression for the minimum-distance decision rule as discussed above has been derived in [15], and for $M = 8$ is given by

$$i^* = \arg \max_{\mathrm{i}\in\{0,\ldots,7\}} \left(\mathrm{R_i}, \mathrm{R_{total}} - \mathrm{R_i} - 3\gamma\mathrm{A}\right), \qquad (6)$$

where i^* is an indicator variable with the following mapping from i^* to data bits: $0 \rightarrow 000$, $1 \rightarrow 001$, ... , $7 \rightarrow 111$.

For practical implementation, since γ (and thus γA) is normally unknown to the receiver, the term γA in (6) can be estimated using $\gamma A \approx R_{\max}$ because $R_{\max}$ would correspond to an ON signal value at the receiver. With this approximation, the decision rule for symbol detection, which is used in this work for both simulation and hardware experiments, becomes

$$i^* \approx \arg \max_{\mathrm{i}\in\{0,\ldots,7\}} \left(\mathrm{R_i}, \mathrm{R_{total}} - \mathrm{R_i} - 3\mathrm{R_{max}}\right). \qquad (7)$$

3. SIMULATION RESULTS FOR DETECTION ERRORS

3.1 Simulation Setup

Consider adjacent LED lamps on the ceiling of height H above the floor and separated by distance L. The receiver is at a fixed height h above the floor, moving horizontally while detecting its position based on the optical power received from LED lamps. Fig. 6 illustrates the LEDs and the receiver together with their coordinates.

The path loss from LED k to the receiver's PD is based on the widely used Lambertian emission model, and is expressed as [7, 8]

$$\gamma_k = \begin{cases} \frac{\kappa(m+1)}{d_k^2}\cos^m\varphi_k \cos\psi_\mathrm{k}\,, & \left|\psi_\mathrm{k}\right| \le \mathrm{FoV} \\ 0, & \text{otherwise} \end{cases} \qquad (8)$$

where κ is the constant including the PD surface area and optical-to-electrical conversion factor, m is the Lambertian order of the emitted light (the higher the

***Table 1**: System parameters for simulation.*

System parameter	Value
PPM/IPPM modulation order (M)	8
PPM/IPPM timeslot duration	0.2 ms
Receiver's sampling rate	25 kHz
Number of bits for position	12
Ceiling height (H)	2 m
LED lamp separation (L)	1.5 m
Receiver height (h)	0.5 m
Lambertian emission order (m)	1
Proportionality constant (κ)	1
Receiver's field of view (FoV)	75°
SNR below each LED lamp	20 dB

more focused), d_k is the distance from LED k to the PD, φ_k is the angle of irradiance from LED k, and ψ_k is the angle of incidence at the PD with respect to LED k, and FoV is the receiver's field of view. Note that the Lambertian emission pattern in (8) is used for performance evaluaton in simulation experiments only. The proposed detection process works regardless of the specific emission pattern. In particular, for hardware experiments in a later section, commercial LEDs that in general do not exactly have a Lambertian pattern are used.

Denote the position of LED k by $\left(X_k, H\right)$, where $X_1 = 0$ and $X_2 = L$ from Fig. 6. When the receiver is at position (x, h), the values of d_k, $\cos\varphi_k$, and $\cos\psi_k$ in (8) can be computed as follows. Note that κ, m, and FoV depend on hardware specifications, and not on the receiver position.

$$d_k = \sqrt{\left(X_k - x\right)^2 + (H - h)^2} \tag{9}$$

$$\cos\varphi_k = \cos\psi_k = \frac{H - h}{d_k} \tag{10}$$

In addition, since $-90^\circ \le \psi_k \le 90^\circ$ in Fig. 6, the condition $|\psi_k| \le$ FoV in (8) can be checked through the equivalent condition $\cos\psi_k \ge \cos(\text{FoV})$.

Table 1 lists system parameter values for simulation experiments. Note that AWGN is such that the Signal-to-Noise Ratio (SNR) when the receiver is directly below each LED lamp is 20 dB. Each LED lamp can be at either the low or high illumination level, yielding a total of four light dimming scenarios. Each numerical data point is a result of 100 simulation runs with randomly generated LED position numbers. Simulation experiments are carried out using the GNU Octave software [18].

3.2 Detection Errors for Different Illumination Scenarios

Fig. 7 shows the error percentages in detecting position numbers at receiver position $(x, 0.5)$ as the receiver moves from position $(0, 0.5)$ to $(1.5, 0.5)$ when both LED 1 and LED 2 are at at the low illumination level.

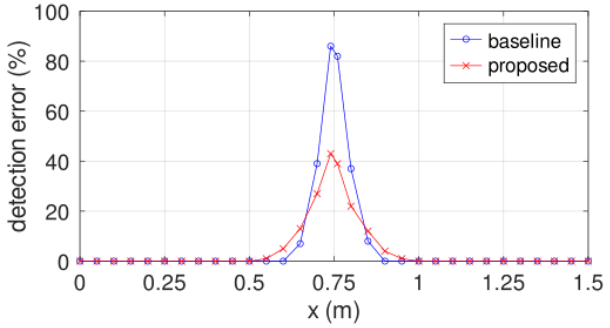

***Fig. 7**: Detection errors for LED 1 and LED 2 at the low illumination level.*

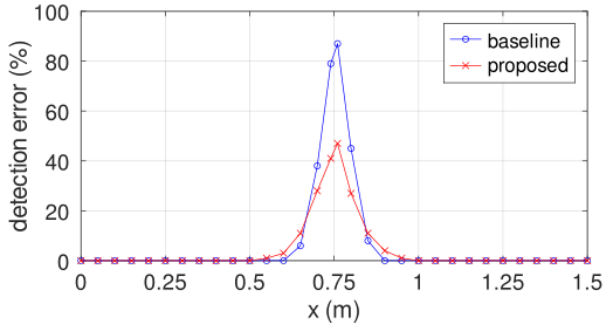

***Fig. 8**: Detection errors for LED 1 and LED 2 at the high illumination level.*

The baseline and proposed plots are without and with interference mitigation through timeslot-interleaved TDM, respectively. Since interference is strongest at the midpoint $(0.75, 0.5)$, the error percentage reaches its peak at this position for each plot. Observe that interference mitigation in the proposed scheme can help reduce the error percentages, in particular from approximately 80% to 40% around the midpoint position. Similar results can be observed from Fig. 8 when both LED 1 and LED 2 are at the high illumination level.

Fig. 9 shows the error percentages when LED 1 is at the low illumination level while LED 2 is at the high illumination level. Higher error percentages for $x < 0.75$ m (compared with $x > 0.75$ m) indicate the asymmetry of the scenario. In particular, positions under low illumination ($x < 0.75$ m) are affected by strong interference from the LED at the high illumination level. The benefit of the proposed interference mitigation is clearly demonstrated for x in the range $[0.35, 0.6]$ m, where the baseline case without TDM suffers from much higher error percentages.

The opposite trend can be observed in Fig. 10 when LED 1 is at the high illumination level while LED 2 is at the low illumination level. For x in the range $[0.9, 1.15]$ m, the baseline case without TDM suffers from much higher error percentages. From Fig. 9–10, the use of TDM can reduce the position interval with error percentages above 10% from approximately 0.5 m to approximately 0.25 m.

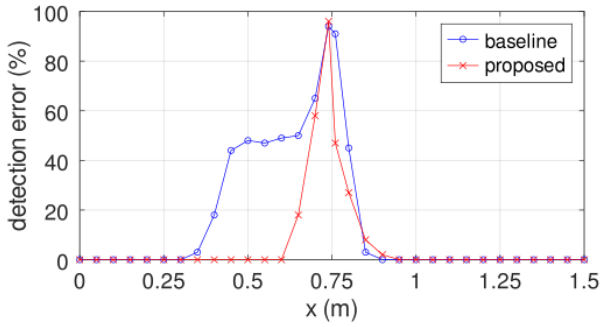

***Fig. 9**: Detection errors for LED 1 and LED 2 at the low and high illumination levels, respectively.*

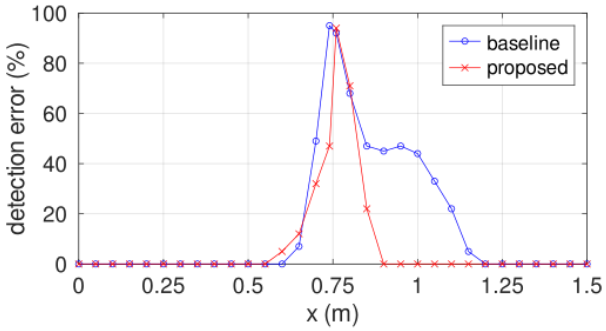

***Fig. 10**: Detection errors for LED 1 and LED 2 at the high and low illumination levels, respectively.*

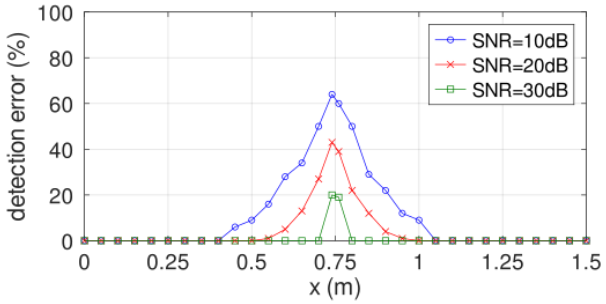

***Fig. 11**: Detection errors for LED 1 and LED 2 at the low illumination level for SNR = 10, 20, 30 dB.*

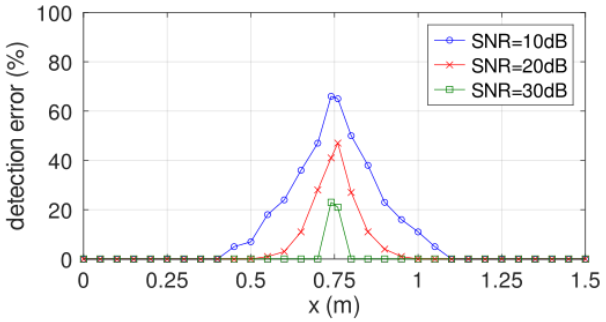

***Fig. 12**: Detection errors for LED 1 and LED 2 at the high illumination level for SNR = 10, 20, 30 dB.*

In summary, numerical results from simulation experiments indicate that interference mitigation with timeslot-interleaved TDM can help reduce detection error percentages, especially when the dimming levels of adjacent LED lamps are different.

3.3 Detection Errors for Different SNRs

To investigate the effects of the SNR on the detection performance, detection errors are evaluated at different SNRs in this section. The SNR levels of 10, 20, and 30 dB are selected for high, medium, and low noise levels, respectively. Note that the results in the previous section correspond to the medium noise level with SNR = 20 dB.

Fig. 11 shows the error percentages when both LED 1 and LED 2 are at the low illumination level, i.e., using 8-PPM, for different SNRs. As expected, the low SNR (10 dB) leads to highest error percentages while the high SNR (30 dB) leads to lowest error percentages. Note that, despite the high SNR, frame header detection errors caused mainly by signal interference among adjacent LEDs can still happen around the midpoint. Recall that the use of timeslot-interleaved TDM can reduce signal interference but does not completely remove it.

Fig. 12 shows the error percentages when both LED 1 and LED 2 are at the high illumination level, i.e., using 8-IPPM, for different SNRs. Compared to Fig. 11, similar results can be observed, indicating that the detection error performance remains the same regardless of the illumination level.

3.4 Errors Based on Multiple Detections

To explore how detection error percentages can be reduced around the midpoint between adjacent LEDs for a given SNR level, this section demonstrates the use of multiple detection results instead of a single detection result. In particular, considering using three successive detection results as follows. If three detected position numbers are the same, then the number is taken as the final result. Otherwise, take the two most frequently detected numbers and conclude that the receiver is between the two LEDs associated with those two position numbers. If the two detected numbers match the two LED position numbers, then the conclusion is counted as a correct detection.

Fig. 13 shows the error percentages around the midpoint when both LED 1 and LED 2 are at the low illumination level with and without considering multiple detections. Numerical results indicate that using multiple detections and allowing for in-between conclusions can reduce the error percentages significantly. Fig. 14 shows the error percentages when both LED 1 and LED 2 are at the high illumination level with and without multiple detections. The same reduction in error percentages can be observed. While the use of multiple detections improves the detection performance, it increases the detection delay for positioning.

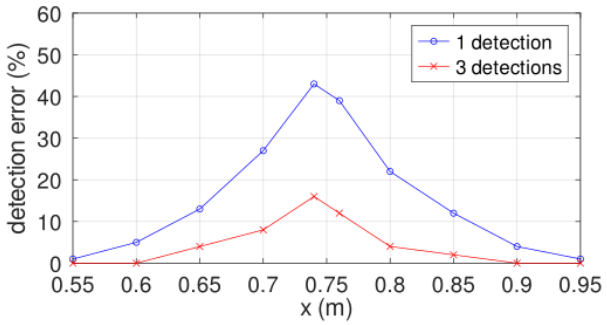

***Fig. 13**: Detection errors for LED 1 and LED 2 at the low illumination level for SNR = 20 dB with and without multiple detections.*

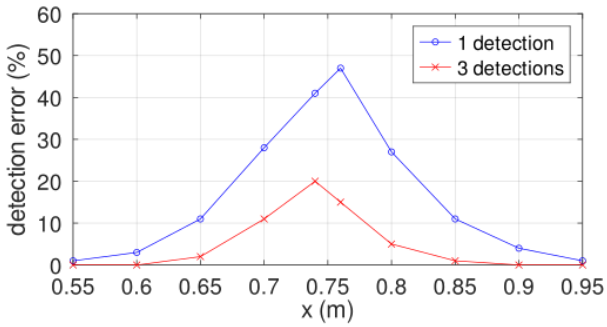

***Fig. 14**: Detection errors for LED 1 and LED 2 at the high illumination level for SNR = 20 dB with and without multiple detections.*

4. HARDWARE EXPERIMENTS

This section describes hardware implementation and experiments of a proximity-based indoor VLP system. Fig. 15 shows the laboratory environment for the test system with three LED lamps. Each LED lamp is made using a Cree XLamp CMA1306 LED chip. Similar to Table 1, LED lamps are 2 m from the floor, and are separated by 1.5 m. In addition, the receiver is 0.5 m from the floor. For performance evaluation, the receiver moves from LED 1 towards LED 3.

Fig. 16 shows the transmitter circuitry for signal modulation and LED switching. A Terasic DE0-CV FPGA development board is used for signal modulation. In particular, three 8-PPM/IPPM signals with timeslot-interleaved TDM are generated, one for each LED lamp. For TDM, LEDs 1 and 3 transmit data in the same timeslots while LED 2 transmits in the other timeslots. These signals are fed to IRLZ44N MOSFETs to switch LEDs on and off accordingly. The position numbers of LEDs 1, 2, and 3 are set to be 101, 102, and 103, respectively.

Fig. 17 shows the receiver circuitry for detection of a position number. An OSRAM SFH206K module is used as a PD. It produces a photocurrent that is proportional to the intensity of the received optical signal. This photocurrent is amplified using a LM358 op-amp module. The amplified signal is then fed to

***Fig. 15**: Test area for system demonstration and performance evaluation.*

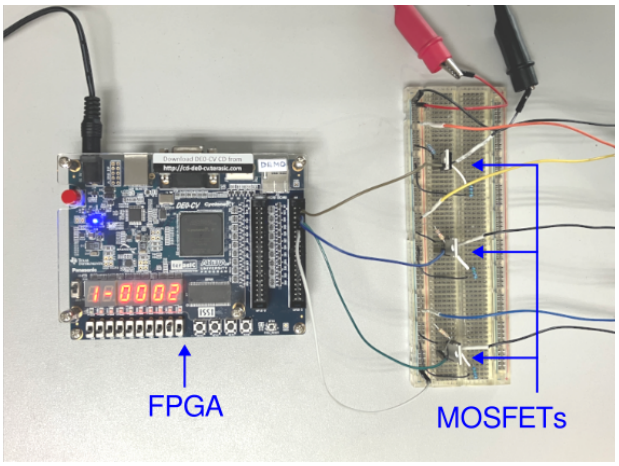

***Fig. 16**: Transmitter circuitry for signal modulation and LED switching.*

the Analog-to-Digital Converter (ADC) input of a RPI-PICO-WH microcontroller module that performs signal processing for detection of a position number according to the decision rule in (7). The detected position number is fed to a laptop computer for display.

Fig. 18 shows example detections of position numbers 101 and 102 under LEDs 1 and 2, respectively. In the figure, the receiver is located roughly directly below each LED lamp. Detection errors become more common at positions between LED lamps, as evaluated next.

Fig. 19 shows the detection error percentages for different values of horizontal coordinate x in receiver position $(x, 0.5)$. Note that the receiver positions right below LEDs 1, 2, and 3 are $(0, 0.5)$, $(1.5, 0.5)$, and $(3, 0.5)$, respectively. Each data point is based on 50 consecutive detections of the position number at the same position. In addition, there are two illumination scenarios in Fig. 19, namely all LEDs at the high illumination level, and all

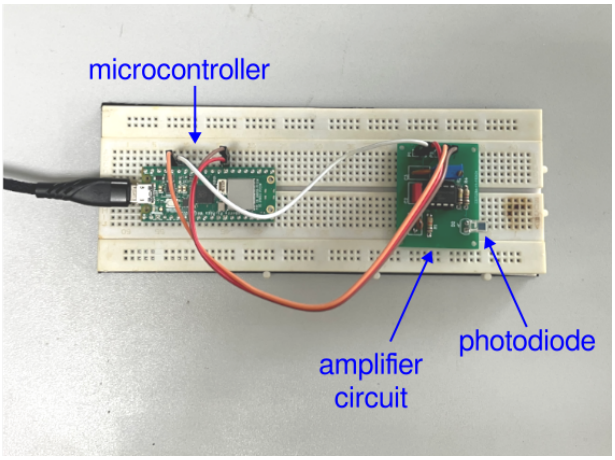

***Fig. 17**: Receiver hardware for signal reception, amplification, and processing.*

***Fig. 18**: Demonstration of detecting position numbers 101 and 102 under LEDs 1 and 2.*

LEDs at the low illumination level.

As expected, in Fig. 19, high error percentages appear around $x = 0.75$, which is the midpoint between LEDs 1 and 2. Similarly, high error percentages appear around $x = 2.25$, which is the midpoint between LEDs 2 and 3. Based on the results, between each pair of adjacent LEDs, there is a section of approximately 0.2 m with significantly higher detection error percentages compared to the remaining positions. It is worth noting that, since actual hardware modules are always different, the detection error percentages are not symmetric around the middle position (1.5, 0.5) in Fig. 19.

Similar to Fig. 19, Fig. 20 shows detection error percentages for different values of x. However, the illumination levels are not the same for all LED lamps. In particular, two scenarios are considered. In the first scenario, LED 2 (in the middle) is at the low illumination level while the others are at the high illumination level. In the second scenario, LED 2 is at the high illumination

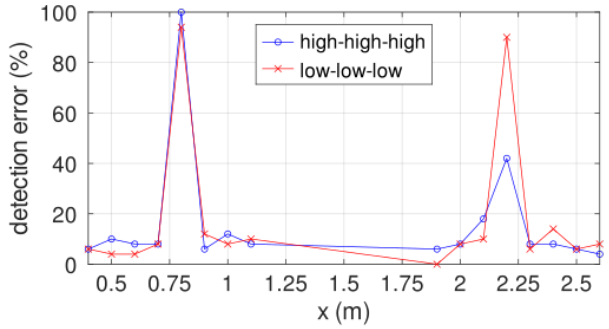

***Fig. 19**: Detection errors from hardware experiments using three LED lamps at the same illumination level.*

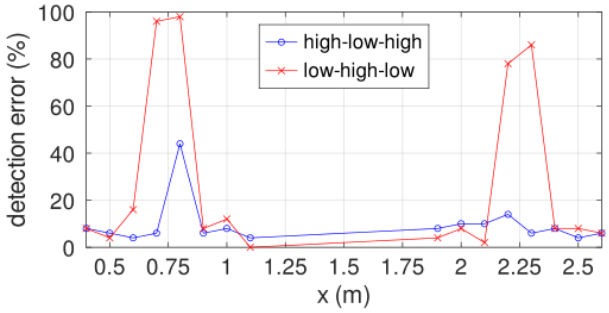

***Fig. 20**: Detection errors from hardware experiments using three LED lamps at different illumination levels.*

while the others are at the low illumination level.

Similar to Fig. 19, in Fig. 20, high detection errors appear around $x = 0.75$ and $x = 2.25$, which are the midpoints between adjacent LED lamps. Compared to the scenarios with the same illumination levels for all LED lamps, the sections with high detection error percentages around $x = 0.75$ and $x = 2.25$ are found to be approximately 0.3 m, which are wider than 0.2 m in Fig. 19.

Note that there is a noise floor for detection error percentages in both Fig. 19 and Fig. 20. Reduction of this noise floor is a subject for future investigation. One possibility is to increase the LED brightness for higher SNRs. Another approach is the use of error control coding to handle bit errors.

Fig. 21 compares detection error percentages from hardware experiments to those from simulation experiments with SNR = 20 dB. Four cases of illumination levels are considered, with each LED at either low or high illumination level. While the error percentages from hardware and simulation experiments do not match closely, the same error trends can be observed, with peak error percentages close to the midpoint between two LEDs. Note that, due to hardware inconsistencies in realistic scenarios, e.g., unequal transmit optical powers from LEDs, peak error percentages are not exactly at the midpoint between two LEDs for hardware experiments.

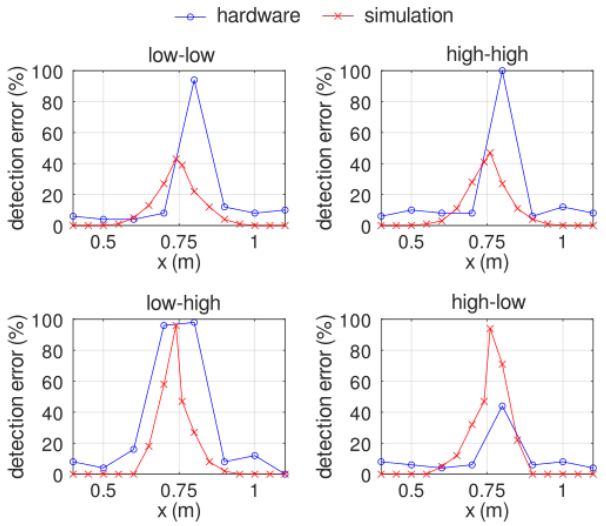

Fig. 21: Detection errors from hardware and simulation experiments (with SNR = 20 dB) for the four cases of illumination levels for LED 1 and LED 2.

5. CONCLUSION

This work introduced the dimming feature to proximity-based indoor VLP systems by using a combination of PPM and IPPM for the low and high illumination levels, respectively. In addition, to mitigate signal interference between adjacent LED lamps, timeslot-interleaved TDM was adopted. Simulation results show that TDM can help reduce detection errors. In particular, an indoor scenario in which LED lamps are 1.5 m apart on the ceiling of height 2 m is considered, with the receiver 0.5 m above the floor and the SNR below each lamp equal to 20 dB. When the two LED lamps are at the same illumination level, TDM can reduce the detection error percentages around the midpoint approximately from 80% to 40%. For different illumination levels, TDM does not reduce peak errors at the midpoint but shortens the position interval with errors above 10% from approximately 0.5 m to approximately 0.25 m.

Then, a hardware demonstration system was developed using the proposed dimmable PPM/IPPM scheme with timeslot-interleaved TDM. Experimental results indicate that position numbers can be successfully detected at most receiver positions, except at positions around midpoints between adjacent LED lamps. Finally, flexible dimming with different illumination levels for adjacent LED lamps was shown to be possible at a cost of widening position intervals with high detection error percentages above 20% approximately from 0.2 m to 0.3 m.

Practical limitations of the developed system include the need to have line-of-sight paths between LED lamps and the receiver. More specifically, the user needs to face the receiver unit, in particular the PD detection area, up towards the ceiling in order to receive data signals from LED lamps. Another limitation is the assumption of LED lamps along the walkway. For LED lamps on the ceiling of a large auditorium, two-dimensional arrangements of LED lamps should be investigated. Finally, the use of PPM/IPPM with timeslot-interleaved TDM assume time synchronization between adjacent LED lamps, which becomes an additional requirement for system implementation.

Suggested future works include scaling up the system and evaluating the detection performance with more LED lamps in a larger space, including two-dimensional LED arrangements in a large hall. In such a setting, user mobility tracking over time can be demonstrated through a visualization dashboard or a screen attached to the receiver unit. In addition, the use of adaptive signal processing algorithms based on machine learning techniques to reduce detection errors can be explored, in particular for dynamic scenarios in which background light changes and signal blockages occur occasionally. Finally, for a battery-operated receiver unit, incorporation of an energy harvesting unit, e.g., a solar cell, can also be investigated.

ACKNOWLEDGEMENT

This research project was financially supported by Thailand Science Research and Innovation (TSRI). The project was under the Fundamental Fund (FF) for the fiscal year of 2025, with the project number 4790426.

REFERENCES

[1] J. Armstrong, Y.A. Sekercioglu, and A. Neild, "Visible light positioning: A roadmap for international standardization," *IEEE Communications Magazine*, vol. 51, no. 12, pp. 68–73, Dec. 2013.

[2] M.F. Keskin, A.D. Sezer, and S. Gezici, "Localization via visible light systems," *Proceedings of the IEEE*, vol. 106, no. 6, pp. 1063–1088, June 2018.

[3] A.B.M.M. Rahman, T. Li, and Y. Wang, "Recent advances in indoor localization via visible lights: A survey," *Sensors*, vol. 20, no. 5, Mar. 2020.

[4] S. Bastiaens, M. Alijani, W. Joseph, and D. Plets, "Visible light positioning as a next-generation indoor positioning technology: A tutorial," *IEEE Communications Surveys & Tutorials*, vol. 26, no. 4, pp. 2867–2913, 4th Quarter 2024.

[5] JEITA, *Visible Light Beacon System*. JEITA Standard CP-1223, May 2013.

[6] IEEE, *IEEE Standard for Local and Metropolican Area Networks–Part 15.7: Short-Range Optical Wireless Communications*. IEEE Standard 802.15.17-2018: 2018.

[7] N. Chi, *LED-Based Visible Light Communications*. Springer, 2018.

[8] V. Vappangi, V.V. Mani, and M. Sellathurai, *Visible Light Communication*. CRC Press, 2021.

[9] F. Zafar, D. Karunatilaka, and R. Parthiban, "Dimming schemes for visible light communication: The state of research," *IEEE Wireless Communications*, vol. 22, no. 2, pp. 29–35, Apr. 2015.

[10] T. Wang, F. Yang, J. Song, and Z. Han, "Dimming techniques for visible light communications for

human-centric illumination networks: State-of-the-art, challenges, and trends," *IEEE Wireless Communications*, vol. 27, no. 4, pp. 88–95, Aug. 2020.

[11] R. Lee et al., "Performance analysis of *M*-ary PPM in dimmable visible light communications," in *Proceedings of the 5th International Conference on Ubiquitous and Future Networks (ICUFN)*, Da Nang, Vietnam, 2013.

[12] K. L. Sterckx and P. Saengudomlert, "Visible light communications via dimmable LED lamps," in *Proceedings of the 16th European Conference on Networks and Optical Communications (NOC)*, Newcastle upon Tyne, UK, 2011.

[13] S. Das and S. K. Mandal, "Dimming controlled multiheader hybrid PPM (MH-HPPM) for visible light communication," *Optical and Quantum Electronics*, vol. 53, no. 2, Feb. 2021.

[14] F. Fang, S. Xiao, Z. Chen, and W. Hu, "Shaped polar codes for dimmable visible light communication," *Optics Communications*, vol. 496, Oct. 2021.

[15] P. Saengudomlert and K.L. Sterckx, "Pulse position modulation with flexible dimming support for visible light communication," *APSIPA Transactions on Signal and Information Processing*, vol. 12, no. 1, Oct. 2023.

[16] P. Saengudomlert and P. Ubolkosold, "Joint position and orientation estimation for visible light positioning using extended Kalman filters," in *Proceedings of the 21st International Conference on Electrical Engineering/Electronics, Computer, Telecommunica-tions and Information Technology (ECTI-CON)*, Khon Kaen, Thailand, 2024.

[17] P. Saengudomlert, P. Ubolkosold, and K.L. Sterckx, "Development of a position and orientation estimation system using extended Kalman filtering for indoor visible light positioning," *AEUE International Journal of Electronics and Communications*, vol. 192, pp. 155684, Jan. 2025.

[18] GNU, *GNU Octave: Scientific Programming Language*, octave.org/index.html.

Poompat Saengudomlert obtained the B.S.E. degree in Electrical Engineering from Princeton University, USA, in 1996. He then obtained the S.M. and Ph.D. degrees, both in Electrical Engineering and Computer Science, from Massachusetts Institute of Technology (MIT), USA, in 1998 and 2002 respectively. From 2003 to 2004, he was a Postdoctoral Research Associate in Laboratory of Information and Decision Systems (LIDS) at MIT. From 2005 to 2013, he was a faculty member in Telecommunications at Asian Institute of Technology (AIT), Thailand. From 2013 to present, he is an Associate Professor in Telecommunication Engineering at Bangkok University's Center of Research in Optoelectronics, Communication and Computational Systems (BU-CROCCS), Thailand. His research interest includes visible light communications, communication theory, and network optimization.

Karel Sterckx, a Belgian national, received a Master of Applied Engineering in Electrical and Electronic Engineering from a college that is currently part of Catholic University Leuven (Belgium) in 1986. In 1997, he obtained a Master of Science in Optoelectronics and Communications Systems from Northumbria University (UK) and, in 2000, a Ph.D. from Swansea University (UK) for work on infrared wireless communication links. He has experience as a practicing engineer in the Belgian audio-visual industry, and has been lecturing at colleges and universities in Thailand since 1993. He has been a resident of Thailand for over 30 years and joined Bangkok University in 2010 as Research Scholar. Since 2012, he is the director of the Bangkok University Center of Research in Optoelectronics, Communications and Computational Systems (BU-CROCCS). His research efforts concentrate on broadband indoor Optical Wireless Communication and Software Defined Communication Systems.

Nutthakun Wannaprapa is a fourth-year undergraduate student majoring in Computer and Robotics Engineering at Bangkok University. His academic interests include embedded systems, signal processing, and smart environments. He is currently conducting research on indoor object tracking using LED lighting for his senior project.